

Nanoscale

Accepted Manuscript

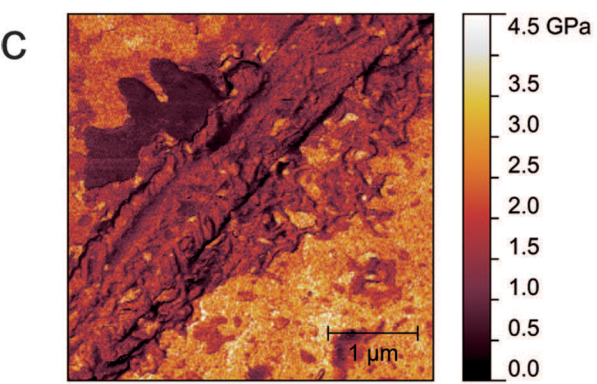
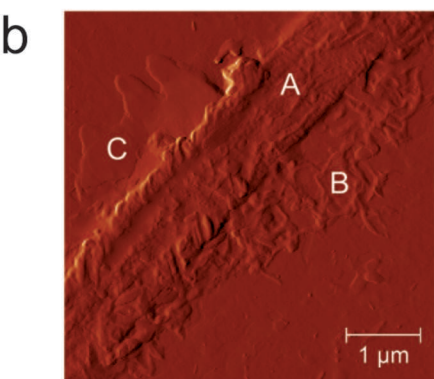
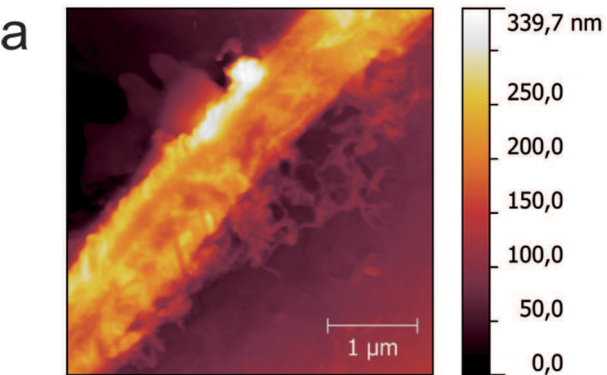


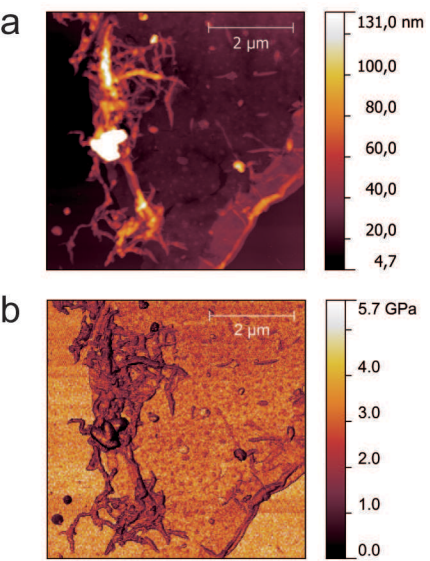
This is an *Accepted Manuscript*, which has been through the Royal Society of Chemistry peer review process and has been accepted for publication.

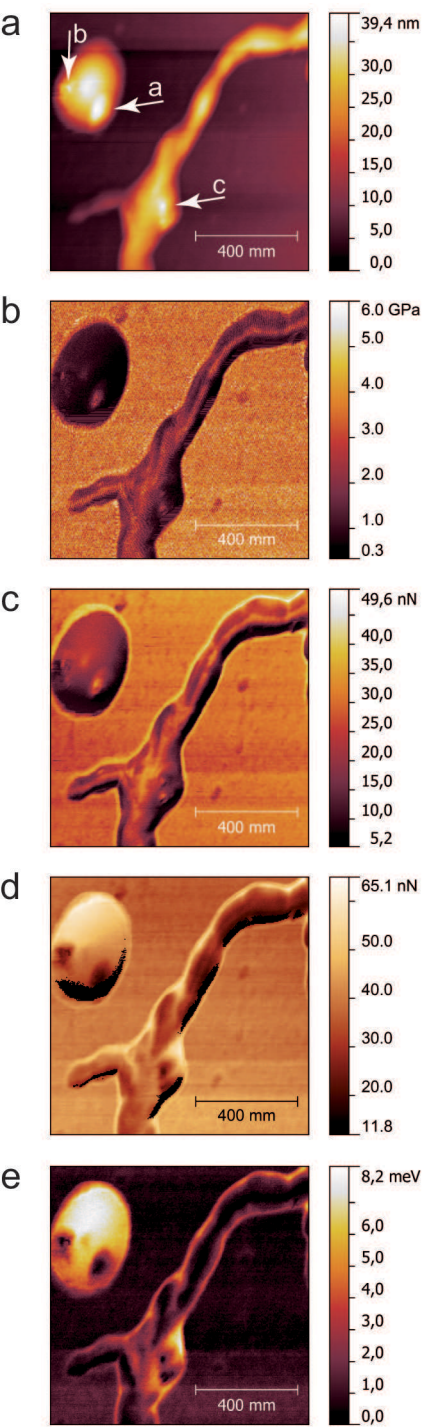
Accepted Manuscripts are published online shortly after acceptance, before technical editing, formatting and proof reading. Using this free service, authors can make their results available to the community, in citable form, before we publish the edited article. We will replace this *Accepted Manuscript* with the edited and formatted *Advance Article* as soon as it is available.

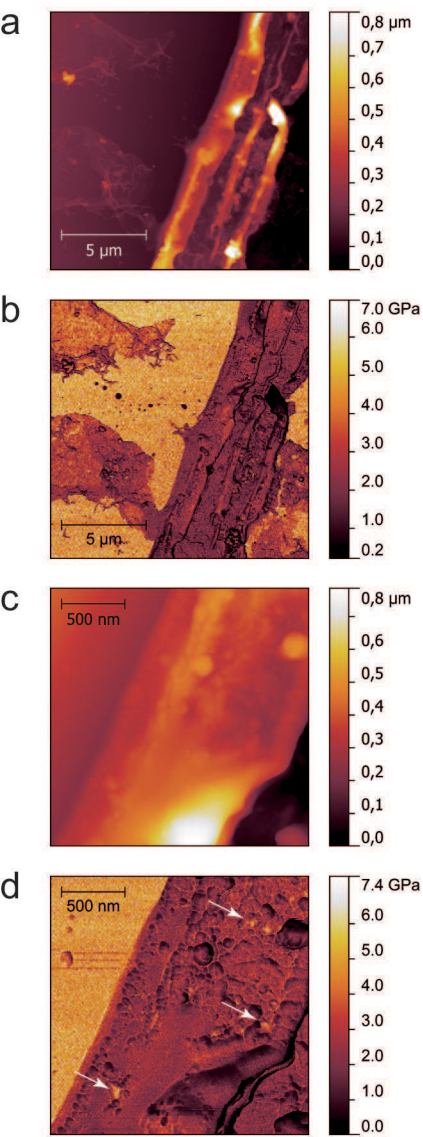
You can find more information about *Accepted Manuscripts* in the [Information for Authors](#).

Please note that technical editing may introduce minor changes to the text and/or graphics, which may alter content. The journal's standard [Terms & Conditions](#) and the [Ethical guidelines](#) still apply. In no event shall the Royal Society of Chemistry be held responsible for any errors or omissions in this *Accepted Manuscript* or any consequences arising from the use of any information it contains.

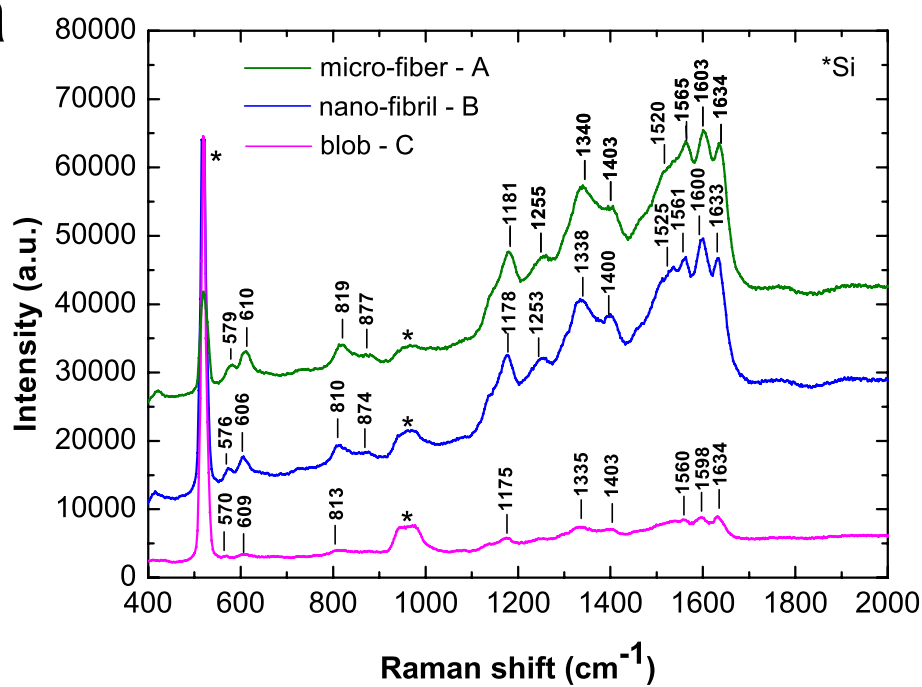




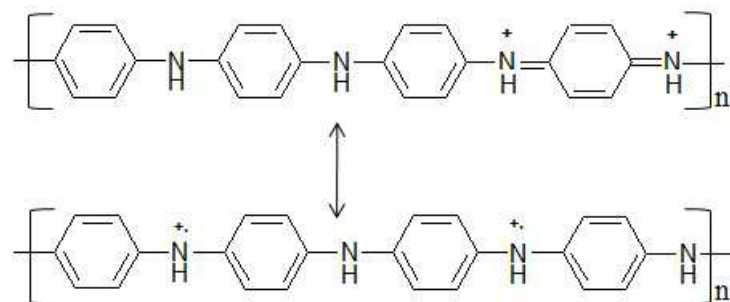




a



b



Polyaniline-nanodiamond fibers as the
self-assembling of nano-fibrils: a
nanomechanical study

Daniele Passeri ^{*a}, Emanuela Tamburri^b, Maria Letizia
Terranova^b, and Marco Rossi^{a,c}

^aDepartment of Basic and Applied Sciences for Engineering,
SAPIENZA University of Rome, Via A. Scarpa 16, 00161 Rome,
Italy

^bDepartment of Chemical Sciences and Technologies, University
of Rome Tor Vergata and Micro and Nano-structured Systems
Laboratory (MINASlab), Via della Ricerca Scientifica, 00133
Rome, Italy

^cResearch Center for Nanotechnology applied to Engineering of
SAPIENZA University of Rome (CNIS), Piazzale A. Moro 5,
00185 Rome, Italy

*Corresponding author: daniele.passeri@uniroma1.it

Abstract

Based on atomic force microscopy (AFM), torsional harmonics atomic force microscopy (TH-AFM, also referred to with the commercial name HarmoniXTM) allows one to perform quantitative characterization of the mechanical properties of soft samples at the nanometer scale. In this work, such a technique has been employed to study the mechanical properties of self-assembled micrometrical fibers of polyaniline (PANI) doped with nanodiamond (ND) particles and to investigate the role of ND in the assembly. In particular, besides PANI-ND fibers, other features, i.e., nano-fibrils and blobs, have been observed on the sample, the mechanical properties of which have been determined and compared after correcting for the effect of the substrate and of the cylindrical geometry of nano-fibrils. Their similar mechanical properties suggest that PANI-ND micro-fibers are constituted by self-assembly of nano-fibrils. Finally, the combination of nanomechanical characterization with energy dispersive X-Ray (EDX) and Raman analysis allowed us to determine that softer blobs are residuals of amorphous PANI not polymerized in nano-fibrils.

Keywords: Atomic force microscopy - polyaniline fibers - nanodiamond - mechanical properties - torsional harmonics atomic force microscopy

1 Introduction

Due to their possible applications in different technological fields, e.g., in sensors and actuators, conductive polymers in form of either films or fibers have been extensively studied [1–5]. Among other conductive polymers, physical and chemical properties have been investigated of polyaniline (PANI) in form of either films or fibers [6–8]. As for others polymers, advances in PANI technology have been obtained by doping with nanomaterials in order to enhance the mechanical and/or electrical properties of the resulting nanocomposite [9–11]. This requires the availability of experimental methods to test the mechanical properties of the obtained nanocomposite materials through different length scales, i.e., from meso- down to nanometer scale [12]. Depth-sensing indentation is a standardized technique effective and accurate for bulk samples and films on substrates, in the latter case providing that the film is thick enough. In case of microscopic materials, such as the case of nanocomposite PANI fibers, specific methods have to be developed. For example, Singh et al. [13] set up a tensile testing tool operating in a scanning electron microscope in order to study the overall elastic properties of one dimensional microstructures. Several methods either (quasi)static or dynamic based on atomic force microscopy (AFM) have been developed due to the possibility of such a tool of probing the sample with accurate nanometrical control of the position using a tip with a radius of a few nanometers [14, 15]. Such techniques are necessary for example in case the mechanical properties of the samples have to be investigated at locations on the samples selected with nanometrical spatial resolution, when an issue is the uniformity of the mechanical properties on the sample, or when the effects on the sample of the presence of nanosized features is under investigation. Among such techniques, torsional harmonics AFM (TH-AFM) allows one to collect quantitative maps of sample indentation modulus, cantilever peak force, tip-sample adhesion and dissipation during a indentation cycle [16, 17].

In a recent study, we used TH-AFM to characterize the elastic modulus of nanocomposited fibers synthesized by chemical polymerization of PANI in presence of detonation nanodiamond (ND) nanoparticles [18]. By examining thoroughly the morphology of the sample, though, we observed the presence of amazing nanometer scale features (nano-fibrils). In this work, we focus the attention to these nano-fibrils: by accurate characterization of their mechanical properties and the comparison with the those of the other features visible on the sample (i.e., the PANI-ND fibers and some amorphous

structures similar to blobs) we deduced the role of nano-fibrils in the formation of the microscopic fibers and the effect of the presence of ND particles on the elastic properties of the nanocomposite.

2 Torsional harmonics atomic force microscopy

In standard tapping mode AFM on soft materials, the tip periodically indents the surface of the sample at the frequency f_1^0 of the first resonance mode of the cantilever. Consequently, the cantilever deflection signal contains the information about one force-distance curve periodically repeated at each cycle of tapping and thus at the frequency f_1^0 of the tapping itself. In principle, force-distance curves could be extracted by analyzing the deflection signal by inverse Fourier transform. Nevertheless, while the frequency response of the cantilever can be considered flat below f_1^0 , the presence of the higher flexural modes of the cantilever distorts the spectrum above f_1^0 , which complicates the extraction of the force-distance curves. To overcome such limitation, in TH-AFM a T-shaped cantilever is used with a out-of-axis tip [16, 17]. During the tapping, torsion of the cantilever are excited, enhanced by its shape. Analogously to the deflection signal, the periodic cantilever torsional signal can be analyzed to extract force-distance curve. Indeed, the torsional frequency response of the cantilever can be considered flat below the first torsional resonance frequency t_1^0 of the cantilever which significantly higher than f_1^0 . Thus, the harmonic components of the spectrum are not distorted and can be used to obtain the force-distance curve after inverse Fourier transform and proper filtering, also due to the higher signal-to-noise ratio of the torsional response with respect to the flexural one [16, 17]. Force-distance curves can be analyzed to obtain complete loading and unloading force-indentation curves. The unloading portion of the curves are analyzed using the Derjaguin-Muller-Toporov (DTM) model [19, 20] to obtain the indentation modulus of the sample M , defined as $M = E/(1 - \nu^2)$ for isotropic materials, being E and ν the Young's modulus and the Poisson ratio of the sample, respectively. Force-indentation curves can be used to evaluate also: the maximum force exerted on the sample (F_{\max}) during the indentation, namely the peak force; the force needed to separate the tip from the sample surface during the tip retraction, namely the pull-off force or the tip-sample adhesion (F_{adh}); the energy dissipated during one loading-unloading cycle (E_{diss}). Taking advantage of high speed data acquisition,

such parameters can be evaluated at each point of the scanned area and thus mapped simultaneously to the morphological reconstruction.

3 Experimental

3.1 Samples description

The synthetic procedure of preparation and the detailed characterization of PANI-ND fibers is reported elsewhere [11]. Briefly, PANI-ND fibers were obtained by precipitation polymerization of the aniline monomer in presence of ND particles (with size of 4 – 5 nm) in aqueous solution using ammonium persulfate as radical initiator. An anionic surfactant, i.e., sodium dodecyl sulfate (SDS), was used to facilitate the ND dispersion in the reaction environment. Notably, in the same conditions but in absence of ND no fibers were obtained. PANI-ND fibers were collected on Si single crystals, which served only as flat substrates for AFM characterization and did not participate to their synthesis. The obtained sample mainly resulted in a tightly woven network of belts with length up to some hundreds of microns, width of a few microns and height from hundreds of nanometers up to one micron [11].

3.2 Equipment

TH-AFM was performed in air and at room conditions using an AFM setup (Dimension Icon, Bruker Inc. featuring HarmoniX™) equipped with a T-shaped cantilever with out-of-axis tip (HMX10, Bruker Inc.), with first free flexural resonance in air $f_1^0 = 54.2$ kHz and first free torsional resonance in air $t_1^0 = 964$ kHz. In addition to the sample topography and phase image which are the typical images collected in AFM standard tapping mode, TH-AFM allows one to collect with high resolution images of sample indentation modulus, maximum force applied by the cantilever during indentation (peak force), tip-sample adhesion, and energy dissipation during an indentation. The collected images have been converted into quantitative maps of these parameters following the calibration procedure supplied by the manufacturer. Forces were calibrated on a clean Si single crystal. Indentation images of indentation modulus were calibrated using a blend of polystyrene (PS) and low density polyethylene (LDPE) reference sample (PS/LDPE by Bruker Inc.) with known mechanical properties, i.e., the indentation moduli

of PS and LDPE being $M_{\text{PS}} = 2 \text{ GPa}$ and $M_{\text{LDPE}} = 100 \text{ MPa}$, respectively. In particular, PS is used as the reference for the calibration while LDPE is used as a control material. As detailed in the following Section, it is worth noting that to obtain the indentation modulus maps force-distance curves are fitted using the DMT model [19,20]. Therefore, in case the DMT modulus is not adequate to describe the tip-sample interaction, indentation modulus maps have to be further manipulated in the post-experiment data analysis. To verify the stability of the tip and the accuracy of our measurements, the calibration of the indentation modulus was checked at the end of the measurement session by repeating the analysis of the PS/LDPE sample. Notably, we observed only a negligible increase of 3% between the values of M_{PS} measured at the beginning and at the end of the measurement session which is ascribable to a slight increase in the tip radius due to abrasion. Therefore, in the data analysis we assumed the tip stable during the whole experiment. Local compositional and structural properties of the different features observed on the sample have been studied on selected areas using both scanning electron microscopy (SEM) coupled with energy dispersive X-ray (EDX) analysis and Raman spectroscopy. SEM/EDX characterization has been carried out using a CrossBeam[®] Workstation (FIB-SEM) AURIGA from Carl Zeiss Microscopy equipped with a Quantax EDX system using an XFlash 6 silicon drift detector with a resolution of 121 eV. Elemental analysis has been performed by EDX using electrons at 4 keV, in order to limit as much as possible the electron penetration depth and the spot radius which, in our experimental conditions, were 200 nm and 100 nm, respectively. Raman studies were performed by using a XploRA ONE[™] Raman Microscope (Horiba Jobin Yvon) using a 532 nm excitation laser light and a 1200 gr mm^{-1} grating spectrometer coupled with an air-cooled scientific CCD.

4 Results and discussion

AFM morphological characterization of the PANI-ND sample reveals the presence of three different features, which are all visible in Fig. 1a (topography) and Fig. 1b (error signal). Although the area reported in Fig. 1 is only $4 \times 4 \mu\text{m}^2$, it is representative of the whole sample as the same features (with the same mechanical properties) have been observed all over the sample surface. Significant images of this sample with large field of view cannot be acquired with AFM as the maximum area which can be imaged usually

does not exceed $100 \times 100 \mu\text{m}^2$ due to limitations in the displacement of the AFM scanner along the two directions of the plain. Overview images of the sample obtained with optical and electron (both scanning and transmission) microscopy can be found in our previous work [11]. Mainly, the sample consists in tightly woven network of long belts with length up to some hundreds of microns, width of a few microns and height from hundreds of nanometers up to one micron, one of which is marked with A in Fig. 1b. In addition, networks are visible which are constituted by nano-fibrils with height of 20 nm and length from hundreds of nanometers up to $1 \mu\text{m}$ (marked with B in Fig. 1b). Closer views of PANI-ND fibers reveal that these result from the assembly of such nano-fibrils. Finally, blobs of not structured material are also visible (marked with C in Fig. 1b), with height approximately equal to that of nano-fibrils (20 nm). The indentation modulus map (Fig. 1c) reveals that these three features correspond to different values of indentation modulus. In particular, all the three features are distinguishable from the (stiff) substrate. Fibers and nano-fibrils have approximately the same elastic modulus, while the blobs are significantly more compliant. It is worth noting that the modulation of the topography results in artifacts in the elastic modulus maps, produced by the modulation of the actual tip-sample contact area. This effect is particularly pronounced in correspondence of the sides of fibers and nano-fibrils as well as in correspondence of holes and relieves on overall flat areas. Therefore, quantitative analysis of the images have been carried out considering only the points on the axis of nano-fibrils and selecting areas relatively flat of blobs and fibers on the basis of the topographical images. Analogous values of indentation modulus have been measured on isolated areas of nano-fibrils such as the one shown in Fig. 2a (topography) and Fig. 2b (indentation modulus).

Fig. 3 reports a complete TH-AFM characterization of a nano-fibril and a blob. In particular, the figure shows the topography (Fig. 3a) together with the quantitative maps of indentation modulus (Fig. 3b), peak force F_{max} (Fig. 3c), adhesion force F_{adh} (Fig. 3d), and dissipated energy E_{diss} (Fig. 3e). All the mechanical images coherently indicate that the nano-fibril is significantly stiffer than the blob, as in correspondence of the former higher indentation modulus and peak force are observed. Notably, these two parameters are strictly related, i.e., the bigger the indentation modulus, the bigger the peak force. Indeed, in TH-AFM the images are acquired maintaining constant the amplitude of the cantilever oscillation, like in standard tapping mode. A stiff material is hardly indented and therefore large values of max-

imum deflection (and thus large peak forces) are observed. Conversely, on a compliant sample large indentations occur and thus lower peak force values will be detected. An opposite contrast is observed in the adhesion and dissipation images. Indeed, soft materials are likely to be viscous resulting in larger values of pull-off force and dissipated energy. As expected, the contrast in elastic modulus (Fig. 3b) and peak force (Fig. 3c) maps is the same and is opposite to that in the adhesion (Fig. 3d) and dissipation (Fig. 3e) images. In particular, the nano-fibril shows lower tip-sample adhesion and dissipation, which suggests that the blob is more viscous than the nano-fibril. Notwithstanding this overall behavior, a few spots on the blob (two of which are marked with a and b in Fig. 3a) are stiffer than the surrounding material being all their mechanical properties similar to those of the Si substrate. For the sake of completeness, it should be also noted that analogous spots can be observed on the nano-fibril (one of which is marked with c in Fig. 3a), although some uncertainty in their exact identification arises from the lower contrast with the nano-fibril which is stiffer than the blob. Such features are compatible with stiff ND particles (or more probably small agglomerates of ND particles) emerging from the surface of nano-fibril and blob or buried immediately under it. Analogous stiff spots can be observed also in fibers, as reported in Fig. 4 which shows the topography (Fig. 4a) and the indentation modulus map (Fig. 4b) of a fiber. The topography of a detail of the fiber is reported in Fig. 4c together with the corresponding indentation modulus map (Fig. 4d). In the latter figure, arrows indicate some spots stiffer than the fiber. A definitive interpretation cannot be derived, because such stiff features cannot be reliably characterized by TH-AFM. Indeed, differently from other techniques which combine AFM and ultrasonic methods, e.g., contact resonance AFM [21,22] or ultrasonic force microscopy [23] which allow the analysis of broader ranges of elastic modulus, i.e, from stiff coatings to polymers and cells [24–31], TH-AFM relies on the sample indentation by the tip and therefore it can be used only on soft materials. Although its use up to materials with modulus of 10 GPa such as HOPG was reported [17], from a practical point of view the range is limited by the saturation of the detected moduli which depends on the actual experimental conditions. For example, in the modulus maps reported in this work the Si substrate corresponds to an indentation modulus of about 5 GPa (instead of the expected 165 GPa). Therefore, we cannot consider accurate measured values of elastic modulus as high as 5 GPa. This prevent us to quantitatively characterize the mechanical properties of the bright spots (as well as of the Si substrate) as

they correspond to saturated values of indentation modulus. Nevertheless, on the basis of the previously reported considerations these features can be associated to ND particles emerging from (or buried immediately under) the surface of the fiber.

In order to quantitatively evaluate the indentation modulus of the three features, different areas of the sample have been analyzed. By averaging the obtained results, the indentation modulus of fibers, nano-fibrils, and blobs have been measured as high as 1.60 ± 0.1 GPa, 1.9 ± 0.2 GPa, and 0.8 ± 0.1 GPa, respectively. The reported elastic modulus values were obtained by averaging those obtained for the single features in each AFM image and, then, by averaging the results obtained for different features observed in the same or in different AFM images. In particular, we analyzed: six different fibers (in six different images); one isolated nano-fibril; two areas of nano-fibrils (in different images) in correspondence of which the elastic modulus was obtained as the average value of several nano-fibrils; four blobs. On the same feature, the modulus was obtained by averaging: from some points (pixels of the images) to a few tens of points of the image in the case of nano-fibrils, which were selected in correspondence of the top of the nano-fibril in order to avoid artifacts arising from the contact between the side of the tip and the edge of the nano-fibril; from some tens to a few hundreds of points in correspondence of blobs, depending on the size of the feature; a few hundreds of points in correspondence of each fiber, which was possible due to their larger area. In the case of blobs and fibers, the areas for the evaluation of the elastic modulus were selected in the center of the features so that they could be considered almost flat on the basis of the topographical images, in order to avoid topography-induced artifacts in the elastic modulus maps. It is worth noting that the error in the reported values represents a standard deviation of the mean from repeated measurements. The evaluation of the uncertainty in our technique is not straightforward, as in practically all the AFM-based techniques for the characterization of physical parameters (e.g., mechanical, electric, or magnetic) at the nanometer scale. Indeed, the uncertainty is mainly affected by the sample topography. For example, the roughness alters the actual tip-sample contact area which modifies the apparent elastic modulus even in case of uniform mechanical properties. Thus, the roughness is expected to increase the dispersion of data, i.e., the standard deviation of the measurements. Also, the tilt angle of the sample surface alters the apparent contact stiffness even in case of uniform and perfectly flat surface as the tip-sample contact is not perfectly normal [32], which induces a bias in

the measured values. Thus, a realistic evaluation of the uncertainty should include considerations on the roughness and tilt of the surface. Due to the difficulties in this calculation, we carried out an evaluation of the ‘minimal’ uncertainty which characterizes our technique on our almost perfectly flat PS/LDPE reference sample, expecting nevertheless a bigger uncertainty on the actual samples. The evaluation of all the partial uncertainties is difficult because, to the best of our knowledge, certified reference materials (CRMs) are not available for mechanical characterizations at the nanometer scale. The sample more similar to a CRM is the PS/LDPE reference material. We verified that the value of indentation modulus of PS of 2 GPa reported by the vendor is pretty accurate using standardized mechanical tests. Conversely, the value of 100 MPa for the indentation modulus of LDPE islands is more difficult to verify with other techniques because the LDPE regions in the PS matrix are only a few tens of nanometers deep. Thus, different techniques sensitive to the properties of the material down to different depths under the surface will give different values as a consequence of the effect of the PS substrate (to the best of our knowledge, TH-AFM is the technique with the smaller penetration depth) [14]. In order to calculate the contribution to the uncertainty given by the reproducibility, we analyzed the measurements on the same PS/LDPE reference sample randomly performed over a four-year period (from 2011 to 2015) by different operators. We measured $M_{\text{LDPE}} = 97.0 \pm 6.5$ MPa in good agreement with the value reported by the vendor. The contribution to the uncertainty (type A) from the reproducibility is therefore equal to $\pm 7\%$, which therefore represents the minimum value of uncertainty we must expect in our measurements. Also, we must consider an additional contribution from the drift the reference values of the elastic modulus of PS equal to $\pm 1.5\%$. Therefore, in our measurements we cannot expect a uncertainty smaller than $\pm 8.5\%$, which is likely to increase depending on the sample roughness. Interestingly, for the three features on our sample the actual values of error are $\pm 10\%$, $\pm 9\%$, and $\pm 8\%$ for blobs, fibers and nano-fibrils. The measured values of indentation modulus retrieved from the as obtained indentation modulus maps (M_{meas}) are reported in Table 1. It is worth noting that the comparison among the values of M_{meas} is not straightforward as the three features have different shape and thickness. Indeed, while fibers and blobs can be considered as films, being their lateral dimensions much bigger than those of the tip, nano-fibrils have much more limited lateral dimensions. To evaluate the actual shape of nano-fibrils and to rationalize the results of TH-AFM nanomechanical characterization, the

actual tip radius R_t was evaluated. Indeed, having performed several images of the PS-LDPE reference sample before starting the measurement session on PANI-ND fibers, we observed a constantly increase in the (not calibrated) signal proportional to the elastic modulus of the two polymeric phases. Since such a signal is proportional to the tip radius, this result reveals an increase in the value of R_t . The measurements on the PANI-ND fibers sample have been performed only when the signal (and thus the tip radius) was stable between subsequent images. Therefore, TH-AFM images have been carried out using a tip with a radius larger than the nominal one for a brand new tip which does not exceed 10 nm. It is well known that AFM morphological images are actually the convolution between the real morphology of the sample and the tip shape [33, 34]. In case of big features like the PANI-ND fibers, it has an almost negligible influence in the reconstruction of the fiber morphology as only fine details are affected by the tip-surface convolution. Conversely, in case of nanometer scale objects, the lateral dimensions are highly affected by the tip shape. Generally, the tip radius can be evaluated, for instance, by imaging standard reference samples with inverted arrays of tips [35]. These samples allow one to reconstruct the shape of the tip up to about 500 nm from the apex. This is important in case of AFM based depth sensing indentation performed on soft materials when a few hundred nanometer penetration depths are reached [36, 37]. Conversely, values of penetration depth reached in TH-AFM do not exceed a few nanometers. Therefore, the knowledge of the only curvature radius of the apex is needed. To evaluate R_t , we analyzed the sections of nanometer features on the sample (i.e., nanometer sized defects which can be found on the Si substrate, particles, residuals, as well as the nano-fibrils themselves). The images of these objects show unrealistically broadened lateral dimensions with respect to their height. Being smaller than the tip, their cross section profile is mainly given by the shape of tip. Therefore, from the cross sections of different nanometer sized objects we evaluated the actual curvature radius of the AFM tip R_t as high as $R_t = 40$ nm. As expected, such a value is bigger than that of a brand new tip, which generally does not exceed 10 nm, as we purposely performed several images before starting the measurement session in order to stabilize the tip. Assuming such a value of R_t , the nano-fibrils can be modeled as cylinders with radius $R_f = 10$ nm. In TH-AFM, indentation modulus maps are automatically obtained using the DMT model and thus a correction must be introduced to obtain the ‘true’ indentation modulus of the nano-fibrils, i.e., to convert the modulus measured on a cylinder into the equivalent inden-

tation modulus of a film on a substrate (M_{fs}). Moreover, as nano-fibrils and blobs are much thinner than the fibers, their measured indentation modulus is expected to be much more affected by the elastic modulus of the stiff substrate. Thus, in order to compare their values with that of fibers, the values of the ‘film-only’ indentation modulus M_f of nano-fibrils and blobs have to be deduced from M_{fs} .

As for the evaluation of M_{fs} of nano-fibrils, according to the DMT model, when a rigid sphere (i.e., the tip) with radius R_t indents the flat surface of a much more compliant material, the tip-sample interaction force F is described by

$$F = \frac{4}{3}M_s\sqrt{R_t}h^{3/2} - F_{adh} \quad (1)$$

where h is the indentation depth. Conversely, if the tip indents a cylinder with radius R_f , the interaction force is described by

$$F = \frac{16}{9}M_s\sqrt{R_{eq}}h^{3/2} - F_{adh} \quad (2)$$

being $R_{eq} = \sqrt{R_t^2 R_f / (R_t + R_f)}$ [38]. By comparing Eqs. (1) and (2), the real indentation modulus value M_{fs} can be deduced from the apparent M_{meas} one through the relation

$$\frac{M_{fs}}{M_{meas}} = \frac{3}{4}\sqrt[4]{\frac{R_t + R_f}{R_f}} \quad (3)$$

Substituting the values of $R_t = 40$ nm and $R_f = 10$ nm, the value $M_{fs} = 2.1 \pm 0.4$ GPa is obtained for the nano-fibrils (Table 1).

In order to correct the effect of the different values of thickness, the ‘film-only’ indentation modulus M_f of nano-fibrils and blobs can be roughly estimated from the values of F_{max} and F_{adh} obtained in Fig. 3c and 3d, respectively. Indeed, the contact radius a_{DMT} at the maximum penetration depth can be evaluated as [39]

$$a_{DMT} = \sqrt[3]{\frac{3(F_{max} + F_{adh})R_t}{4M_{fs}}} \quad (4)$$

and maximum penetration depth as

$$h = \frac{a_{DMT}^2}{R_t} \quad (5)$$

thus obtaining data reported in Table 2. Being the substrate much stiffer than the film, M_f can be evaluated from M_{fs} using the relation

$$M_f = M_{fs} \left(1 - e^{-\frac{\alpha}{r}}\right) \quad (6)$$

where

$$r = \frac{\sqrt{\pi} a_{\text{DMT}}}{2R_f - h} \quad (7)$$

and α is a parameter which depends on the value of r [36, 40, 41]. The actual values of r , α , and the correction factor, i.e., the ratio M_f/M_{fs} for nano-fibrils and blobs are reported in Table 2. Although data reported in Table 2 have been obtained from the detailed analysis of the information retrieved for the single nano-fibril and the single blob in Fig. 3, they allow us to roughly estimate the effect of the geometry and the substrate mechanical properties on the measurements. Indeed, nano-fibrils (blobs) have roughly the same diameter (thickness). Thus, the ratio between the apparent and the effective moduli of blobs and nano-fibrils reported in Table 2 can be used to scale the average apparent elastic modulus values. Finally, the calculated corrected values of M_f for nano-fibrils and blobs are reported in Table 1 and can be compared to that of fibers. One can observe that nano-fibrils and fibers have exactly the same indentation modulus while blobs are much softer. The analysis of the mechanical images and the comparison of the corrected indentation moduli allow one to make out the role of ND particles in the self-assembling of nano-fibrils into fibers and their effect on the mechanical properties of the nanocomposites. Indeed, we must discard the hypothesis that both fibers and nano-fibrils are constituted by the only PANI, as fibers and nanofibrils are not formed in the same conditions of synthesis but in absence of NDs [11, 42]. Also, fibers and nano-fibrils having the same mechanical properties is not compatible with the hypothesis that NDs participate to the formation of fibers but not of nano-fibrils, e.g., that hypothesis that nano-fibrils are made of only PANI while NDs are responsible for the assembly of these nano-fibrils into fibers. Also, NDs are not located on the surface of nano-fibrils and fibers. Indeed, mechanical images indicate that only a few (small agglomerates of) ND particles occasionally emerge from the samples surface. This suggests that NDs are mainly located inside the nanocomposites. On the basis of these considerations, we can deduce that NDs are located inside the single nano-fibril. More specifically, since mechanical properties of nano-fibrils are almost uniform along the same nano-fibril and among different nano-fibrils

and since NDs contribute to nano-fibrils mechanical properties, this suggest that NDs are bound to be located on the nano-fibril axis or close to it. This deduction agrees well with the interpretation of structural characterizations previously reported [11].

Finally, the mechanical properties of soft blobs could be compatible with both traces of amorphous PANI and/or residuals of the surfactant used in the synthesis. In order to elucidate the nature of the soft blobs (which nevertheless represent only a minor and negligible component of the sample), we characterized the three described features through SEM/EDX and Raman analysis. A typical EDX elemental analysis of a PANI-ND fiber is reported in Table 3, which shows that the fibers are characterized by the presence of C and N in a ratio of about 9, higher of but compatible with the value of 6 expected for PANI, and by the presence of residuals from the SDS surfactant. EDX compositional analysis did not show significant differences among fibers, nano-fibrils, and blobs all of which are consequently mainly formed by PANI. In order to rationalize the differences in their elastic modulus, structural analysis has been carried out using Raman spectroscopy. In Fig. 5a the Raman spectra collected on the three typical features highlighted by AFM analysis are reported. The spectroscopic study clearly shows that all three structures, i.e., fiber (marked with A in Fig. 1), nano-fibrils (marked with B in Fig. 1), and blob (marked with C in Fig. 1), are constituted by the polyaniline polymer in its semi-oxidized protonated emeraldine form with the distinctive bands located at about 1340, 1520 and 1600 cm^{-1} [11, 43]. In Table 4 a tentative of assignment of all the Raman bands is reported, while in Fig. 5b the resonant chemical structures referring to the protonated emeraldine form are depicted. It is interesting to note that the peaks attributable to the polymer are well evident in the spectra of fiber and nano-fibrils. On the contrary, the blob produces a spectrum in which not all the characteristic peaks of the polymer are distinguishable, and those present are not particularly resolved. Furthermore, from the fiber, to the nano-fibril, to the blob, the peaks relative to the silicon substrate are gradually more intense. This can be caused by an increase of the sampling depth of the laser radiation due to a lower stability of the sample under the laser irradiation. Effectively, an intense degradation of the blob was observed after spectra acquisition. This occurrence may be explained by a poor packing of the polymer chains, which, inducing a higher amorphous structure, lowers the thermal stability of the material. This phenomenon also suggests that the ND is not embedded into the blob. In fact, previous studies [11, 43, 44] allowed us to highlight how

ND is able to both induce a higher long-range order into the polymer matrix and to increase its thermal stability by decreasing the temperature-induced decomposition of the polymer backbone. Overall, the results of the complementary characterizations indicate that the reduction of elastic modulus in correspondence of blobs is to be ascribed to the fact that they are constituted by amorphous PANI not polymerized as nano-fibrils not embedding ND particles.

5 Conclusion

In conclusion, TH-AFM has been used to perform a nanomechanical study of self-assembly of PANI-ND micro-fibers by analyzing the mechanical properties of three different features observed in the sample, i.e., the micro-fibers themselves, nano-fibrils and blobs. When necessary, the as-measured values of indentation modulus have been corrected to take into consideration the effect of the substrate and that of the cylindrical geometry of nano-fibrils. Our findings allowed us to deduce that ND particles are located inside the nano-fibers, most likely on the axis of the nano-fibrils. Their similar mechanical properties (indentation modulus of about 1.5 GPa) suggest that PANI-ND micro-fibers are constituted by self-assembly of nano-fibrils. Conversely, although in principle are compatible with both amorphous PANI and residuals of surfactant, softer blobs (indentation modulus of about 500 MPa) have been rationalized as residuals of amorphous PANI not polymerized in nano-fibrils through the combination of nanomechanical characterizations with the results of EDX and Raman analysis.

6 Acknowledgements

The authors are grateful to Dr. Francesco Mura for the SEM/EDX analysis.

7 References

- [1] B. Adhikari, S. Majumdar, Polymers in sensor applications, Prog. Polym. Sci. 29 (2004) 699–766.

- [2] L. Groenendaal, F. Jonas, D. Freitag, H. Pielartzik, J. R. Reynolds, Poly(3,4-ethylenedioxythiophene) and its derivatives: past, present, and future, *Adv. Mater.* 12 (2000) 481–494.
- [3] W. A. Daoud, J. H. Xin, Y. S. Szeto, Polyethylenedioxythiophene coatings for humidity, temperature and strain sensing polyamide fibers, *Sens. Actuat. B* 109 (2005) 329–333.
- [4] H. Bai, G. Shi, Gas sensors based on conducting polymers, *Sensors* 7 (2007) 267–307.
- [5] J. Jang, M. Chang, H. Yoon, Chemical sensors based on highly conductive poly(3,4-ethylenedioxythiophene nanorods), *Adv. Mater.* 17 (2005) 1616–1620.
- [6] T. E. Herod, J. B. Schlenoff, Doping-induced strain in polyaniline: stretchoelectrochemistry, *Chem. Mater.* 5 (1993) 951–955.
- [7] H. L. Wang, J. Gao, J. M. Sansiñena, P. McCarthy, Fabrication and characterization of polyaniline monolithic actuators based on a novel configuration: integrally skinned asymmetric membrane, *Chem. Mater.* 14 (2002) 2546–2552.
- [8] A. Mazzoldi, C. Degl’Innocenti, M. Michelucci, D. De Rossi, Actuating properties of polyaniline fibers under electrochemical stimulation, *Mater. Sci. Eng. C Biomim.* 6 (1998) 65–72.
- [9] V. Mottaghitalab, G. M. Spinks, G. G. Wallace, The influence of carbon nanotubes on mechanical and electrical properties of polyaniline fibers, *Synth. Met.* 152 (2005) 77–80.
- [10] Q. Y. Soundararajah, B. S. B. Karunaratne, R. M. G. Rajapakse, Montmorillonite polyaniline nanocomposites: (preparation), characterization and investigation of mechanical properties, *Mater. Chem. Phys.* 113 (2009) 850–855.
- [11] E. Tamburri, V. Guglielmotti, S. Orlanducci, M. L. Terranova, D. Sordi, D. Passeri, R. Matassa, M. Rossi, Nanodiamond-mediated crystallization in fibers of PANI nanocomposites produced by template-free polymerization: Conductive and thermal properties of the fibrillar networks, *Polymer* 53 (2012) 4045–4053.

- [12] R. K. Leach, R. Boyd, T. Burke, H. U. Danzebrink, K. Dirscherl, T. Dziomba, M. Gee, L. Koenders, V. Morazzani, A. Pidduck, D. Roy, W. E. S. Unger, A. Tacoot, The European nanometrology landscape, *Nanotechnology* 22 (2011) 062001.
- [13] R. Singh, D. Paul, R. K. Jain, Biofilms: implications in bioremediation, *Trends Microbiol.* 14 (2006) 389–397.
- [14] D. Passeri, M. Rossi, E. Tamburri, M. L. Terranova, Mechanical characterization of polymeric thin films by atomic force microscopy based techniques, *Anal. Bioanal. Chem.* 405 (2013) 1463–1478.
- [15] F. Marinello, D. Passeri, E. Savio (Eds.), *Acoustic scanning probe microscopy*, Springer Berlin Heidelberg, 2012.
- [16] O. Sahin, S. Magonov, C. Su, C. F. Quate, O. Solgaard, An atomic force microscope tip designed to measure time-varying nanomechanical forces, *Nat. Nanotechnol.* 2 (2007) 507–514.
- [17] O. Sahin, N. Erina, High-resolution and large dynamic range nanomechanical mapping in tapping-mode atomic force microscopy, *Nanotechnology* 19 (2008) 445717.
- [18] D. Passeri, A. Biagioni, M. Rossi, E. Tamburri, M. L. Terranova, Characterization of polyaniline-detonation nanodiamond nanocomposite fibers by atomic force microscopy based techniques, *Eur. Polym. J.* 49 (2013) 991–998.
- [19] B. V. Derjaguin, V. M. Muller, Y. P. Toporov, Effect of contact deformation on the adhesion of particles, *J. Colloid Interface Sci.* 53 (1975) 314–326.
- [20] E. Barthel, Contact, interactions, and dynamics, in: F. Marinello, D. Passeri, E. Savio (Eds.), *Acoustic scanning probe microscopy*, Springer Berlin Heidelberg, 2012, Ch. 2, pp. 21–46.
- [21] U. Rabe, J. Janser, W. Arnold, Vibration of free and surface-coupled atomic force microscope cantilevers: theory and experiment, *Rev. Sci. Instrum.* 67 (1996) 3281–3293.

- [22] K. Yamanaka, A. Noguchi, T. Tsuji, T. Koike, T. Goto, Quantitative material characterization by ultrasonic AFM, *Surf. Interface Anal.* 27 (1999) 600–606.
- [23] F. Dinelli, S. K. Biswas, G. A. D. Briggs, O. V. Kolosov, Measurements of stiff-material compliance on the nanoscale using ultrasonic force microscopy, *Phys. Rev. B* 61 (2000) 13995–14006.
- [24] D. Passeri, A. Bettucci, M. Germano, M. Rossi, A. Alippi, V. Sessa, A. Fiori, E. Tamburri, M. L. Terranova, Local indentation modulus characterization of diamond-like carbon films by atomic force acoustic microscopy two contact resonance frequencies imaging technique, *Appl. Phys. Lett.* 88 (2006) 121910.
- [25] D. Passeri, A. Bettucci, M. Rossi, Acoustic and atomic force microscopy for the mechanical characterization of thin films, *Anal. Bioanal. Chem.* 396 (2010) 2769–2783.
- [26] D. Passeri, M. Rossi, A. Alippi, A. Bettucci, M. L. Terranova, E. Tamburri, F. Toschi, Characterization of epoxy/single-walled carbon nanotubes composite samples via atomic force acoustic microscopy, *Physica E* 40 (2008) 2419–2424.
- [27] D. Passeri, M. Rossi, A. Alippi, A. Bettucci, D. Manno, A. Serra, E. Filippo, M. Lucci, I. Davoli, Atomic force acoustic microscopy characterization of nanostructured Selenium-Tin thin films, *Superlattices Microstruct.* 44 (2008) 641–649.
- [28] A. Kumar, U. Rabe, W. Arnold, Mapping of elastic stiffness in an $\alpha + \beta$ Titanium alloy using atomic force acoustic microscopy, *Jpn. J. Appl. Phys.* 47 (2008) 6077–6080.
- [29] Technique for rapid in vitro single-cell elastography, *Ultrasound Med. Biol.* 32 (11) (2006) 1687–1702.
- [30] P. A. Yuya, D. C. Hurley, J. A. Turner, Contact-resonance atomic force microscopy for viscoelasticity, *J. Appl. Phys.* 104 (2008) 074916.
- [31] D. G. Yablon, A. Gannepalli, R. Proksch, J. Killgore, D. C. Hurley, J. Grabowski, A. H. Tsou, Quantitative viscoelastic mapping of polyolefin blends with contact resonance atomic force microscopy, *Macromolecules* 45 (2012) 4363–4370.

- [32] D. Passeri, M. Rossi, J. J. Vlassak, On the tip calibration for accurate modulus measurement by contact resonance atomic force microscopy, *Ultramicroscopy* 128 (2013) 32–41.
- [33] J. S. Villarrubia, Algorithms for scanned probe microscope image simulation, surface reconstruction, and tip estimation, *J. Res. Natl. Inst. Stand. Technol.* 102 (1997) 425–454.
- [34] F. Marinello, D. Passeri, S. P., E. Savio, Data processing for acoustic probe microscopy techniques, in: F. Marinello, D. Passeri, E. Savio (Eds.), *Acoustic scanning probe microscopy*, Springer Berlin Heidelberg, 2012, Ch. 13, pp. 377–392.
- [35] V. Bykov, A. Gologanov, V. Shevyakov, Test structure for SPM tip shape deconvolution, *Appl. Phys. A* 66 (1998) 499–502.
- [36] D. Passeri, A. Bettucci, A. Biagioni, M. Rossi, A. Alippi, E. Tamburri, M. Lucci, I. Davoli, S. Berezina, Indentation modulus and hardness of viscoelastic thin films by atomic force microscopy: A case study, *Ultramicroscopy* 109 (2009) 1417–1427.
- [37] D. Passeri, A. Alippi, A. Bettucci, M. Rossi, A. Alippi, E. Tamburri, M. L. Terranova, Indentation modulus and hardness of polyaniline thin films by atomic force microscopy, *Synth. Met.* 161 (2011) 7–12.
- [38] K. Sweers, K. van der Werf, M. Bennink, V. Subramaniam, Nanomechanical properties of α -synuclein amyloid fibrils: a comparative study by nanoindentation, harmonic force microscopy, and Peakforce QNM, *Nanoscale Research Letters* 6 (2011) 270.
- [39] M. E. Dokukin, I. Sokolov, Quantitative mapping of the elastic modulus of soft materials with HarmoniX and PeakForce QNM AFM modes, *Langmuir* 28 (2012) 16060–16071.
- [40] A. K. Bhattacharya, W. D. Nix, Analysis of elastic and plastic deformation associated with indentation testing of thin films on substrates, *Int. J. Solids Structures* 24 (1988) 1287–1298.
- [41] R. Saha, W. D. Nix, Effect of the substrate on the determination of thin film mechanical properties by nanoindentation, *Acta Mater.* 50 (2002) 23–38.

- [42] M. Reggente, M. Rossi, L. Angeloni, E. Tamburri, M. Lucci, I. Davoli, M. L. Terranova, D. Passeri, Atomic force microscopy techniques for nanomechanical characterization: A polymeric case study, *JOM* 67 (2015) 849–857.
- [43] E. Tamburri, S. Orlanducci, V. Guglielmotti, G. Reina, M. Rossi, M. L. Terranova, Engineering detonation nanodiamond - polyaniline composites by electrochemical routes: Structural features and functional characterizations, *Polymer* 52 (2011) 5001–5008.
- [44] E. Tamburri, V. Guglielmotti, R. Matassa, S. Orlanducci, S. Gay, G. Reina, M. L. Terranova, D. Passeri, M. Rossi, Detonation nanodiamonds tailor the structural order of PEDOT chains in conductive coating layers of hybrid nanoparticles, *J. Mater. Chem. C* 2 (2014) 3703–3716.

TABLES

Table 1: Mechanical characterization of the features of the PANI-ND sample: fibers (A), nano-fibrils (B) and blobs of polymers (C) not assembled in fibrils. The ‘apparent’ indentation modulus M_{meas} as measured by TH-AFM is reported. The corrected ‘film-substrate’ indentation modulus M_{fs} is reported, where the correction accounts for the cylindrical shape of nano-fibrils and allows one to compare the modulus of nano-fibrils with those of fibers and blobs which can be described as films on the substrate. Finally, the ‘film-only’ indentation modulus M_{f} is calculated in order to compare the modulus of nano-fibrils and blobs (which are affected by the modulus of the substrate) with that of the fibers. Values which do not need correcting are reported in parentheses.

Features	M_{meas} (GPa)	M_{fs} (GPa)	M_{f} (GPa)
Fibers	1.6 ± 0.1	(1.6 ± 0.1)	(1.6 ± 0.1)
Nano-fibrils	1.9 ± 0.2	2.1 ± 0.2	1.5 ± 0.2
Blobs	0.8 ± 0.1	(0.8 ± 0.1)	0.46 ± 0.06

Table 2: Ratio between the indentation moduli of the samples before and after the correction for the substrate effect (M_{fs} and M_f , respectively) and that and parameters used to evaluate it, i.e., maximum tip-sample contact value the contact radius a_{DMT} , the penetration depth h , the parameter r defined in Eq. (7), and the corresponding value of α .

Features	a_{DMT} (nm)	h (nm)	r	α	M_f/M_{fs}
nano-fibrils	9	2	0.89	1.0	0.68
blobs	14	5	1.65	1.4	0.57

Table 3: Typical elemental analysis of a PANI-ND fiber retrieved through SEM/EDX.

Element	Concentration (%)
C	78.4 ± 10.9
O	10.4 ± 3.2
N	8.1 ± 2.9
S	2.6 ± 0.9
Na	0.5 ± 0.2

Table 4: Assignments of the Raman band for the features A (micro-fiber), B (nano-fibrils), and C (blob) illustrated in Fig. 1. Excitation wavelength: 532 nm. (B, benzenoid ring; Q, quinonoid ring; ν stretching; δ , in-plane bending; \sim , bond intermediate between the single and the double bonds; Phz, phenazine-like segment; ^a Wilson notation for aromatic species modes)

Raman shift (cm^{-1})			Assignments
Micro-fiber (A)	Nano-fibrils (B)	Blob (C)	
579	576	570	Phz, B ring def.
610	606	609	ν (C-S), δ (SO ₂)
819	810	813	δ (C-H) _Q (o.p.)
877	874	-	δ (C-H) (o.p.)
1181	1178	1175	δ (C-H) _B
1255	1253	-	ν (C-N) _B
1340	1338	1335	ν (C \sim N ⁺)
1403	1400	1403	Phz
1520	1525	-	δ (N-H) _{SQ}
1565	1561	1560	ν (C-C) _Q , Phz
1603	1600	1598	ν (C-C) _B
1634	1633	1634	ν (C \sim C) _B (8a) ^a , Phz

FIGURES

Figure 1: Typical topography (a), error signal (b), and indentation modulus (c) images obtained on the PANI-ND sample which show the three different features of the sample, i.e., microfibers (A), nanofibrils (B), and blobs (C). Images acquired with Dimension Icon (Bruker Inc.) in HarmoniXTM mode.

Figure 2: Example of an area of the sample where nanofibrils are visible: (a) topography and (b) indentation modulus map. Images acquired with Dimension Icon (Bruker Inc.) in HarmoniXTM mode.

Figure 3: Complete TH-AFM characterization of an area where a nanofibril and a blob are visible: (a) topography, (b) indentation modulus, (c) peak force, (d) adhesion, and (e) dissipation. Arrows in the topography indicate three features compatible with ND particles or small agglomerates emerging from the surface. Images acquired with Dimension Icon (Bruker Inc.) in HarmoniXTM mode.

Figure 4: Topography (a) and indentation modulus (b) of a PANI-ND fiber and topography (c) and indentation modulus (d) of the same fiber at higher magnification. Arrows in (d) indicate features of the maps compatible with ND particles or small agglomerates emerging from the surface. Images acquired with Dimension Icon (Bruker Inc.) in HarmoniXTM mode.

Figure 5: (a) Raman spectra in the spectral range $400 - 2000 \text{ cm}^{-1}$ of fiber, nano-fibrils, and blob (A, B, and C, respectively, as indicated in Fig. 1). (b) Resonant chemical structures of polyaniline semi-oxidized state.